



Response Surface Methodology-optimized Single-batch Production of Herbal Residue-based N,P Co-doped Carbon Materials for Enhanced Electrochemical Efficiency

Sidan Li ^{a,b,c}, Yuzhao Ma,^{a,b,c} Shihua Xu,^{a,b,c} Xueyang Huang,^{a,b,c} Yuehan Li,^{a,b,c} Zheng Li,^{a,b,c} and Yuan Yuan ^{a,b,c,*}

N,P co-doped porous carbon (NPPC) was prepared as a high-performance electrode material for supercapacitors. NPPC materials were synthesized through a facile single-batch carbonization-activation strategy. *Poria cocos* residue was used as a renewable biomass precursor, potassium carbonate as the chemical activator, and melamine phosphate served as the dual N/P doping agent. A Box-Behnken design in response surface methodology was utilized to optimize three critical process parameters: K_2CO_3 ratio, N,P co-doped ratio, and activation temperature, aiming at maximizing the specific capacitance. The morphological, structural, and electrochemical properties of the prepared carbon materials were systematically characterized by scanning electron microscopy, N_2 adsorption–desorption isotherms, X-ray photoelectron spectroscopy, cyclic voltammetry, galvanostatic charge-discharge technique, and electrochemical impedance spectroscopy. The optimized NPPC exhibited hierarchical porous structure with a high specific surface area (reaching $2980\text{ m}^2\cdot\text{g}^{-1}$), uniformly distributed N (12.3 at.%) and P (0.59 at.%) heteroatoms, and excellent supercapacitive performance. It achieved a maximum specific capacitance of $332\text{ F}\cdot\text{g}^{-1}$ at a current density of $1\text{ A}\cdot\text{g}^{-1}$ in a 6 M KOH electrolyte. This work realizes the high-value valorization of TCM solid waste and provides a green, cost-effective, and scalable route for the synthesis of high-performance supercapacitor electrode materials, aligning with the goals of waste recycling and carbon neutrality.

DOI: 10.15376/biores.21.3.6068-6082

Keywords: Herbal residue; Carbon materials; N,P co-doped; Single-batch production; Electrochemical properties; Box–Behnken design

Contact information: a: College of Mechanical and Resource Engineering, Wuzhou University, Guangxi Wuzhou 543000, China; b: Guangxi Engineering Research Center of Comprehensive Utilization of Renewable Resources, Guangxi Wuzhou 543000, China; c: Guangxi University Engineering Research Center of Comprehensive Utilization of Renewable Resources, Guangxi Wuzhou 543000, China;

* Corresponding author: yuan_yuan2014@sina.com

INTRODUCTION

The increasing global energy crisis and the pressing demand for sustainable energy storage solutions have spurred extensive research into high-performance supercapacitors (Jia *et al.* 2025). The heightened interest in supercapacitors stems from their sustainable energy storage potential offering rapid charge–discharge capabilities, long-lasting cycle stability, and eco-friendliness (Zhai *et al.* 2016; Wu *et al.* 2025). The appropriate selection

of electrode materials plays a crucial role in determining electrochemical performance of supercapacitors, and porous carbon materials are emerging as promising candidates due to their large specific surface area, excellent electrical conductivity, and a tunable pore structure (Cheng *et al.* 2024; Qiang *et al.* 2024). Biomass-derived materials are particularly attractive as carbon precursors because of their renewable characteristics, affordability, widespread abundance, and inherent eco-friendliness, all of which align with the goals of waste conversion and carbon neutrality (Yan *et al.* 2017; Tiwari *et al.* 2022; Liu *et al.* 2024; Murugan *et al.* 2024).

Residues from traditional Chinese medicine (TCM) are generated in significant amounts, with China alone producing over 30 million tons annually through decoction processes (Jia *et al.* 2025). Typically, these residues are discarded or incinerated, leading to substantial resource wastage and environmental degradation (Kang *et al.* 2017; Hung *et al.* 2022;). However, these residues are rich in carbonaceous components such as cellulose, hemicellulose, and lignin, and also contain inherent heteroatoms including nitrogen (N) and oxygen (O), making them ideal precursors for producing functional porous carbon materials (Zhou *et al.* 2023; Chen *et al.* 2024). *Poria Cocos* residue (PR) is a widely available, low-cost Chinese herb waste with high carbon content and favorable organic composition for carbonization. It can be readily converted into heteroatom-doped hierarchical porous carbon with large surface area. This can make it a promising precursor for energy storage and environmental applications (Chen *et al.* 2024). Transforming TCM residues into valuable electrode materials can not only address waste disposal problems but also provide a sustainable approach to energy storage (Wang *et al.* 2019).

Common strategies to improve the electrochemical performance of biomass-derived carbon materials include heteroatom doping (such as N, phosphorus (P), sulfur (S)) and chemical activation (Huang *et al.* 2020). Noteworthy, the co-doping of N and P in carbon materials can modify the electronic structure, introduce numerous defect sites, and induce pseudocapacitance through Faradaic redox reactions. This enhancement leads to improved conductivity, wettability, and ion adsorption capabilities (Yan *et al.* 2014; Li *et al.* 2022; Wang *et al.* 2025; Tahir *et al.* 2026). Chemical activation using agents such as potassium hydroxide (KOH) and melamine phosphate is a highly effective strategy for generating hierarchical porous structures specifically comprising micropores and mesopores, which enhance the diffusion of electrolyte ions and optimize the utilization of active sites. Moreover, response surface methodology (RSM) is a valuable tool for optimizing process parameters (Zhang *et al.* 2021; Teimouri *et al.* 2024) such as activation temperature, dopant ratio, and activator dosage, ensuring reproducible and efficient material synthesis (Shi *et al.* 2023).

This is the first study to employ PR as the carbon precursor for N,P co-doped porous carbon (NPPC), realizing the high-value valorization of TCM solid waste and alleviating environmental pollution. A facile single-batch carbonization-activation route was developed using K_2CO_3 as activator and melamine phosphate ($C_3H_9N_6PO_4$) as dual N/P dopant. The single-batch carbonization-activation strategy simplifies the synthetic process, reduces energy consumption, realizes *in-situ* homogeneous heteroatom doping, and avoids intermediate washing/drying steps compared with the traditional two-step method. The Box–Behnken design (BBD) in RSM was utilized to optimize key parameters, including the K_2CO_3 ratio, N and P co-doping ratio, and activation temperature, for specific capacitance. Various techniques were used to characterize the morphological, structural, and electrochemical properties of the materials. To fabricate the working electrode for supercapacitor tests, the optimized NPPC was mixed with acetylene black and

polytetrafluoroethylene (PTFE) at a mass ratio of 8:1:1. As critical components of the electrode, acetylene black serves as a conductive agent to reduce internal resistance and construct efficient electron transport pathways within the electrode matrix, which is consistent with the role of conductive additives in enhancing charge transfer efficiency reported in carbon-based electrode systems (Wang *et al.* 2006). Meanwhile, PTFE functions as a binder to firmly fix the active material (NPPC) and conductive agent (acetylene black) into a coherent and stable structure, preventing particle detachment during electrochemical cycles and ensuring long-term operational reliability of the electrode (Tahir *et al.* 2026).

This study endeavored to establish a practical and sustainable method for transforming TCM residues into high-performance electrode materials for supercapacitors, thereby advancing the generation of environmentally-friendly energy storage systems. This work is the first to fabricate N,P co-doped hierarchical porous carbon from *Poria cocos* residue *via* a single-batch carbonization-activation route optimized by BBD-based RSM. It realizes the high-value conversion of TCM waste and provides a green method for high-performance supercapacitor electrode preparation.

EXPERIMENTAL

Materials

Poria cocos residue (PR) was acquired from a TCM processing factory. PR was first rinsed with purified water to remove impurities, thoroughly dried at 80 °C, and then crushed into fine powder. K₂CO₃, C₃H₉N₆PO₄, HCl, and anhydrous ethanol, were all of analytical purity and were purchased from Guoyao Group Chemical Reagent Co., Ltd. Acetylene black and polytetrafluoroethylene (PTFE, 5 wt.%) were sourced from Dongguan Hongcheng Plastic Raw Materials Co., Ltd. Foam nickel (1 cm × 2 cm, 110 pores per inch, thickness 1.5 mm, 99.9% purity) was procured from Shanghai Yuezhi Electronic Technology Co., Ltd., while nitrogen gas (>99.999% purity) was supplied by Guangzhou Yuejia Gas Co., Ltd.

Synthesis of N,P Co-Doped Porous Carbon Materials

For synthesizing NPPC, aliquots of PR, K₂CO₃, and C₃H₉N₆PO₄ were weighed in varying mass ratios, mixed and ground uniformly, and transferred into a quartz tube as shown in Fig. 1. Single-batch carbonization–activation treatment was conducted under N₂ atmosphere (5 °C·min⁻¹). Specifically, the temperature was raised to 300 °C at a heating rate of 5 °C·min⁻¹ and maintained for 30 min. This is a pre-carbonation stage in a continuous heating process without intermediate cooling, washing or reagent addition. Subsequently, it was further increased to the preset activation temperatures (500 to 700 °C) at a heating rate of 10 °C·min⁻¹ with a holding time of 2 h. After cooling, the obtained products were thoroughly rinsed with dilute HCl and then with purified water until the pH approached neutral. Then, the as-prepared sample was dried at 105 °C for 6 h to obtain the final material, which was denoted as NPPC. For comparative analysis, the sample obtained under only K₂CO₃ activation was used as a control and referred to as PC.

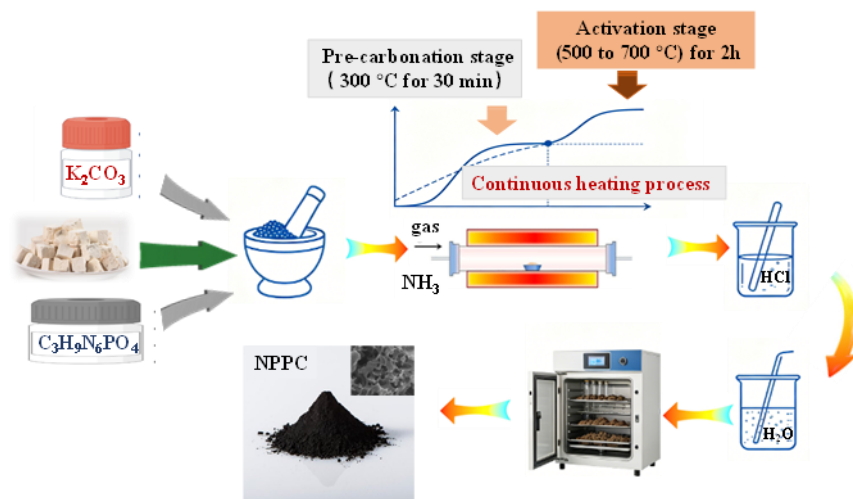


Fig. 1. A schematic diagram of the single-batch synthesis of NPPC

Characterization of Materials

The morphology of the samples was characterized by scanning electron microscopy (SEM, FEI, Hillsboro, The Netherlands). The surface area and pore size distribution of the product were determined by Brunauer–Emmett–Teller (BET) analysis (Quantachrome Autosorb ASAP 2460, USA). The crystal structure of the products was analyzed by X-ray diffraction (XRD, smartlab9, Japan) and Raman spectroscopy (Confocal Laser MicroRaman spectrometer, Horiba LabRAM HR Evolution, Japan). The elemental valence states of the samples were analyzed by X-ray photoelectron spectroscopy (XPS, Thermo Escalab 250xi, USA).

Electrochemical Measurements

For the fabrication of working electrodes for supercapacitor electrochemical measurements, NPPC was mixed with acetylene black and PTFE at a mass ratio of 8:1:1. An appropriate amount of anhydrous ethanol was added dropwise to the mixture while stirring magnetically at 300 rpm for 30 min to form a homogeneous viscous slurry with a solid content of ~25 wt%. The slurry was then subjected to ultrasonic dispersion for 10 min to eliminate agglomerates and to ensure uniform distribution of components. Prior to coating, nickel foam was pre-treated by sequential immersion in 3 M HCl solution for 15 min (to remove surface oxides), deionized water, and anhydrous ethanol for ultrasonic cleaning (each for 10 min), followed by drying at 100 °C for 2 h to ensure surface cleanliness and conductivity. The well-dispersed slurry was uniformly coated onto the pre-treated nickel foam using a microsyringe (100 μ L) with a coating area precisely controlled at 1 cm \times 1 cm. The coated nickel foam was transferred to a vacuum oven and dried at 80 °C for 6 h under a pressure of -0.09 MPa to remove residual solvent and enhance interparticle adhesion. After drying, the electrode was pressed at a pressure of 10 MPa for 30 s using a tablet press to improve the contact between the active material layer and the nickel foam current collector, reducing interfacial resistance. The actual mass loading of NPPC on each electrode was weighed for the nickel foam before and after coating/drying, with an average loading of 4.5 ± 0.2 mg to ensure experimental reproducibility. All electrodes were stored in a desiccator under vacuum prior to electrochemical testing.

The three-electrode tests were conducted on an electrochemical workstation (Chenhua CHI660E), including cyclic voltammetry (CV), galvanostatic charge-discharge

(GCD), and electrochemical impedance spectroscopy (EIS). Among them, the potential window of the CV test was -1 to 0 V, and the scanning rate was 10 to 100 mV/s. The potential window for GCD was -1 to 0 V, and the current density was 1 to 10 A/g. The EIS test was conducted under an open-circuit voltage of 5 mV, with a frequency range of 10 mHz to 100 kHz. The electrode material, which was a platinum sheet, and HgO/Hg electrode were employed as working electrode, counter electrode, and reference electrode, respectively. A 6 M KOH solution was used as electrolyte.

The specific capacitance of the electrode material was calculated by Eq. 1,

$$C = \frac{I \times \Delta t}{m \times \Delta V} \quad (1)$$

where C is the specific capacitance ($\text{F}\cdot\text{g}^{-1}$); I denotes the discharge current ($\text{A}\cdot\text{g}^{-1}$); Δt represents the discharge time (s); m is the mass of the electrode material (g); and ΔV denotes the voltage difference (V).

Experimental Design

A BBD with three independent parameters and three levels was generated using Design-Expert 8.0.6 software (Stat-Ease Inc., Minneapolis, USA). In total, 17 experiments were conducted on a central location to determine the variables that impact specific capacitance. This approach allows for the establishment of statistical relationships between experimental variables and response variables, which can characterize the response surface and determine the optimal manufacturing conditions (Yuan *et al.* 2024). These features can enable the prediction of the optimal board properties. Table 1 presents the design matrix and the specific capacitance values of NPPC.

Table 1. BBD for Coded Factors and Results for Specific Capacitance of NPPC.

| Code | Factors | | Range and Levels | | |
|------|--------------------------------------|----|------------------|---|----------|
| | | | Low (-1) | Medium (0) | High (1) |
| A | K ₂ CO ₃ ratio | | 1 | 2 | 3 |
| B | N,P co-doped ratio | | 0.3 | 0.5 | 0.7 |
| C | Activation temperature (°C) | | 500 | 600 | 700 |
| Run | Factors | | | Specific capacitance ($\text{F}\cdot\text{g}^{-1}$) | |
| | A | B | C | | |
| 1 | -1 | -1 | 0 | 304 | |
| 2 | 0 | 0 | 0 | 331 | |
| 3 | 0 | 0 | 0 | 330 | |
| 4 | 1 | -1 | 0 | 279 | |
| 5 | 0 | 1 | -1 | 267 | |
| 6 | -1 | 1 | 0 | 234 | |
| 7 | 0 | 0 | 0 | 327 | |
| 8 | 1 | 0 | 1 | 302 | |
| 9 | 1 | 0 | -1 | 297 | |
| 10 | 0 | -1 | -1 | 330 | |
| 11 | 0 | -1 | 1 | 278 | |
| 12 | -1 | 0 | 1 | 278 | |
| 13 | 1 | 1 | 0 | 302 | |
| 14 | -1 | 0 | -1 | 292 | |
| 15 | 0 | 0 | 0 | 330 | |
| 16 | 0 | 0 | 0 | 329 | |
| 17 | 0 | 1 | 1 | 298 | |

The specific capacitance of NPPC was affected by three critical parameters: the K_2CO_3 ratio (A), the N,P co-doped ratio (B), and the activation temperature (C). These parameters were selected as independent variables based on preliminary experimental results. An analysis of variance (ANOVA) was conducted at a 95% confidence level. All data were presented by taking the average of three replicates and their coefficient of variations (C.V.s) (Yuan *et al.* 2024). The C.V. observations for the NPPC samples and the PC control sample were found to be consistent.

RESULTS AND DISCUSSION

Data Analysis and Regression Models

Table 2 lists the ANOVA p-values for specific capacitance. All p-values below 0.05 were significant, and those above 0.05 indicated insignificant model terms (Alslaibi *et al.* 2013). Furthermore, p-values below 0.01 suggest that the model for specific capacitance is highly statistically significant, with only a 0.01% probability that these values are a result of random noise. The significant model terms in this scenario included A, B, AB, BC, A^2 , B^2 , and C^2 .

Table 2. Analysis of Variance for Parameters and their Interactions

| Source | Sum of squares | df | Mean square | F-value | P-value |
|-------------|----------------|----|-------------|----------|----------------------|
| Model | 13557.24 | 9 | 1506.36 | 81.29931 | <0.0001 |
| A | 612.5 | 1 | 612.5 | 33.05705 | 0.0007 |
| B | 1012.5 | 1 | 1012.5 | 54.64534 | 0.0002 |
| C | 98 | 1 | 98 | 5.289129 | 0.0550 ^{ns} |
| AB | 2162.25 | 1 | 2162.25 | 116.6981 | <0.0001 |
| AC | 72.25 | 1 | 72.25 | 3.899383 | 0.0889 ^{ns} |
| BC | 1722.25 | 1 | 1722.25 | 92.95104 | <0.0001 |
| A^2 | 3201.603 | 1 | 3201.603 | 172.7927 | <0.0001 |
| B^2 | 3086.55 | 1 | 3086.55 | 166.5833 | <0.0001 |
| C^2 | 834.1289 | 1 | 834.1289 | 45.01852 | 0.0003 |
| Residual | 129.7 | 7 | 18.52857 | | |
| Lack of fit | 58.5 | 3 | 19.5 | 1.095506 | 0.4476 ^{ns} |
| Pure error | 71.2 | 4 | 17.8 | | |
| Cor total | 13686.94 | 16 | | | |

^{ns} Not significant

The regression equation is as follows:

$$\begin{aligned} \text{specific capacitance of NPPC} = & 334.40 + 8.75A - 11.25B - 3.50C \\ & + 23.25AB + 4.25AC + 20.75BC - 27.58 A^2 - 27.08 B^2 - 14.07C^2 \quad (2) \end{aligned}$$

The models were a good fit, with an R^2 values of 0.9905 for all. The predicted R^2 value (0.9235) was consistent with the adjusted R^2 value (0.9783). The Lack of Fit F-value of 1.10 suggested that the model was not significant. The low coefficient of variation (C.V.% = 1.43) validated the accuracy and reliability of the experimental values in the regression model (Yuan *et al.* 2024).

Response Surface Interaction Analysis

Figure 1 exhibits the significant interaction combinations AB and BC that were selected to analyze their interactive effects on the specific capacitance of NPPC. The interaction effect between the K_2CO_3 ratio (A) and N,P co-doped ratio (B) was greater than that between the N,P co-doped ratio (B) and activation temperature (C). Figure 1a illustrates that there was a significant positive synergistic interaction between A and B. The optimization of the K_2CO_3 ratio was able to maximize the specific capacitance only when the N,P co-doped ratio was moderate. Conversely, only when the K_2CO_3 ratio was moderate was the optimization of the co-doping ratio able to achieve the best effect. Moreover, there was also a notable positive synergy between B and C (Fig. 1b). Only when the activation temperature was moderate was the optimization of the co-doping ratio able to maximize the specific capacitance. By contrast, only when the co-doping ratio was moderate was the optimization of activation temperature able to achieve the maximum effect. This indicates that an increase in temperature caused continuous pore opening and expansion in the material, resulting in activated carbon with a well-developed pore structure. However, if the activation temperature is too high, the carbon skeleton may become overly etched, leading to the continuous transformation of micropores into mesopores and macropores. This can also result in the collapse and damage of some pores, negatively impacting the electrolyte ion adsorption and eventually decreasing the specific capacitance.

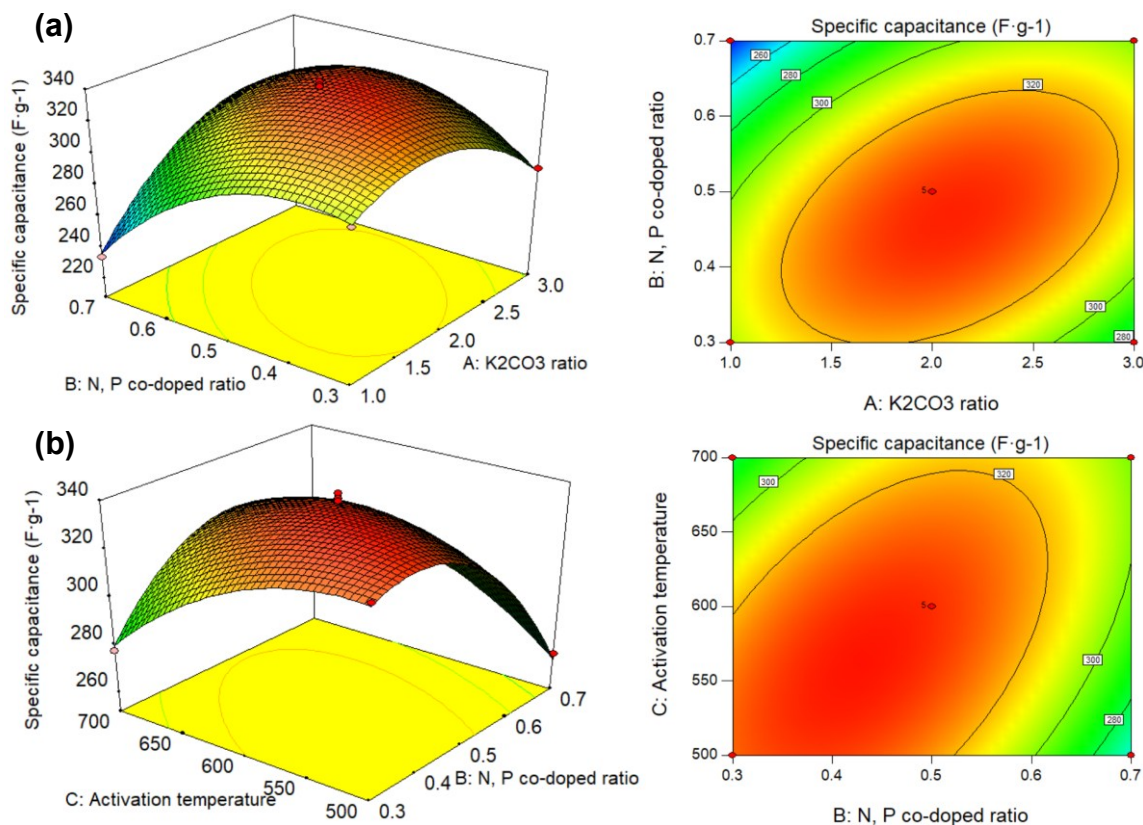


Fig. 1. The response surface plots and response contour plots of (a) interactive effect of K_2CO_3 ratio (A) and N,P co-doped ratio (B) on specific capacitance; (b) interactive effect of N,P co-doped ratio (B) and activation temperature (C) on specific capacitance

Optimization and Verification Experiment

After the optimization analysis was completed, verification experiments were carried out employing the identical methodology under the determined optimal conditions: a K_2CO_3 ratio (A) of 1.97, an N, P co-doped ratio (B) of 0.42, and an activation temperature (C) of 579°C . Under these conditions, the predicted specific capacitance reached $339\text{ F}\cdot\text{g}^{-1}$. The experiment was optimized for convenience by adjusting the process parameters as follows: K_2CO_3 ratio (A) is 2.0, N, P co-doped ratio (B) is 0.4, and activation temperature (C) is 580°C . Under these conditions, the observed NNPC specific capacitance was $332\text{ F}\cdot\text{g}^{-1}$, which shows that the model had high reliability and good reproducibility for the NNPC specific capacitance.

Electrochemical Analysis

Figure 2a exhibits the CV curves of PC, showing narrower integral areas and significant triangular distortion at scan rates $>50\text{ mV}\cdot\text{s}^{-1}$, but at 10 to $10\text{ mV}\cdot\text{s}^{-1}$, the CV curves became more pronounced.

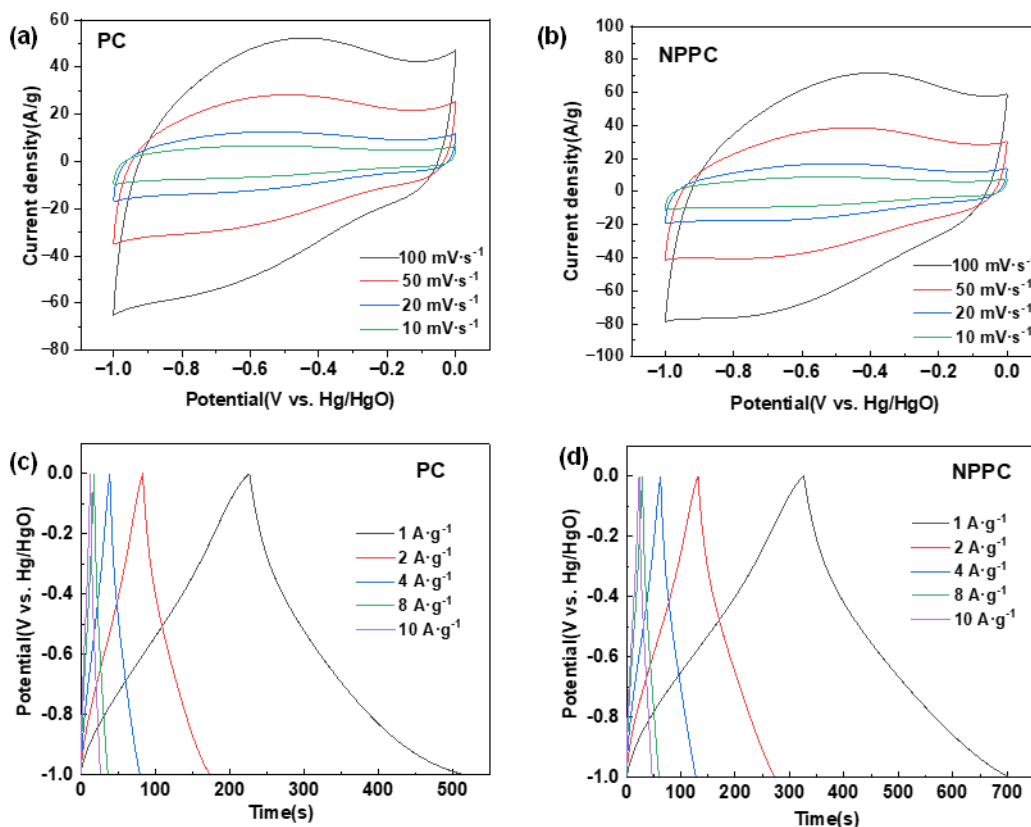


Fig. 2. The responses of (a) PC and (b) NNPC; and GCD profiles responses of (c) PC and (d) NNPC at different current densities

Figure 2b demonstrates that NNPC exhibited nearly rectangular profiles with minimal distortion, even at a scan rate of $100\text{ mV}\cdot\text{s}^{-1}$, suggesting a synergistic integration between electric double-layer capacitance and pseudocapacitance. The capacitance at $1\text{ A}\cdot\text{g}^{-1}$, as determined from GCD tests and depicted in Figs. 2c and 2d, indicates that NNPC achieved a value of $332\text{ F}\cdot\text{g}^{-1}$, which was 1.47 times higher than that of PC ($226\text{ F}\cdot\text{g}^{-1}$).

The minor deviation from an ideal rectangular shape observed at low scan rates can be attributed to Faradaic redox reactions involving pyridinic nitrogen ($N-H_2 \leftrightarrow N+H_2$) and phosphorus-containing groups ($P-O \leftrightarrow P=O$) (Qiang *et al.* 2024).

Figure 3 illustrates that each sample exhibits a high-frequency semicircle related to charge transfer resistance (R_{ct}). The measured series resistance (R_s) values were 0.79Ω for PC and 0.62Ω for NPPC. These R_s values were fairly consistent in both samples, with slight variations possibly due to intrinsic resistance differences in the carbon materials (Chen *et al.* 2025). The R_{ct} values for PC and NPPC were 0.76 and 0.35Ω , respectively. The Warburg resistance (Z_w) in NPPC also exhibited a steeper low-frequency slope, suggesting an accelerated ion diffusion process within the hierarchical porous structure.

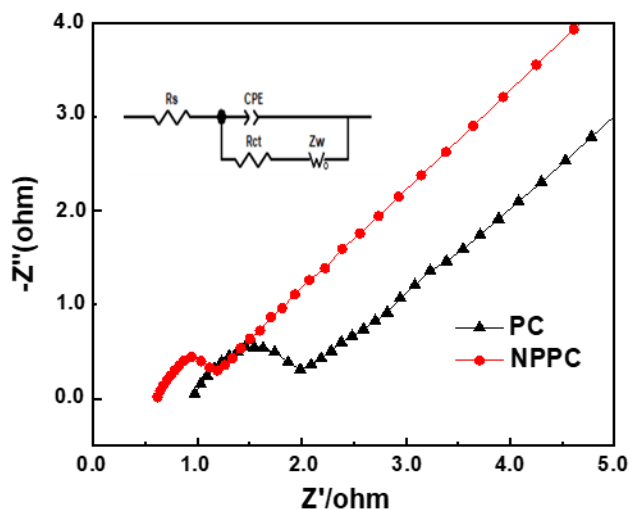


Fig. 3. Nyquist plots of PC and NPPC in 6 M KOH

Morphological and Structural Characteristics

Figures 4(a and b) exhibit SEM images of the synthesized electrode materials, revealing their microscopic morphological characteristics and microstructural evolution. Both the figures show a three-dimensional interconnection framework with a clear porous structure. Figure 4a exhibits a honeycomb-like structure of PC, produced by the pore-forming effect of CO, CO₂, and K, obtained by decomposition of K₂CO₃. The CO and CO₂ can etch carbon to form micropores, while K vapor can get incorporated into the graphene layer, resulting in the disruption of the carbon microstructure (Qiang *et al.* 2024). Comparatively, NPPC shows a large-diameter flower-shaped thin nanosheet structure with C₃H₉N₆PO₄ (Fig. 4b), which is possibly due to the combined effect of physico-chemical double active agents with unique pore-forming capabilities (Wang *et al.* 2025; Liu *et al.* 2026).

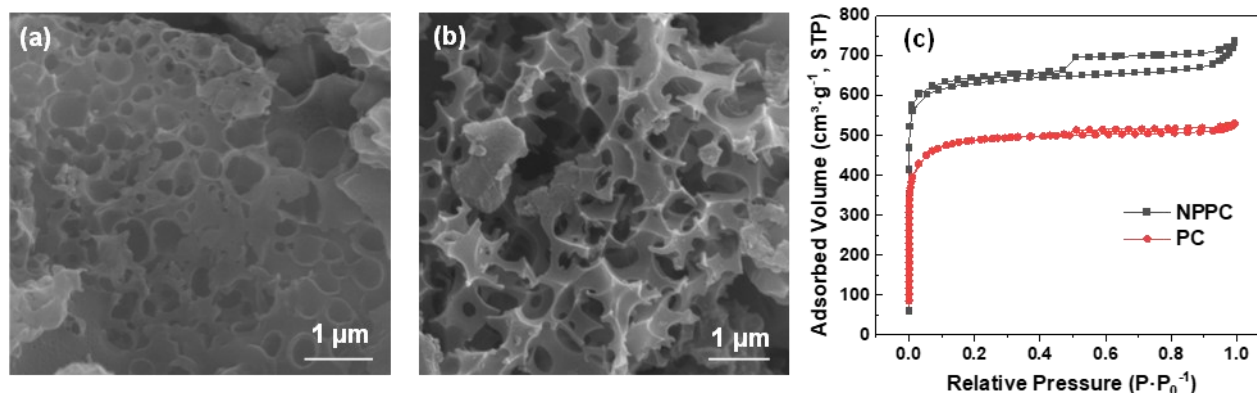


Fig. 4. SEM images of (a) PC and (b) NPPC, and (c) nitrogen adsorption–desorption isotherms of PC and NPPC

As shown in Fig. 4c, NPPC had a hierarchical porous structure (with micropores and mesopores), as evident from the type IV N_2 adsorption–desorption isotherms with distinct hysteresis loops (at $P/P_0 > 0.5$). It exhibited a significantly higher specific surface area (S_{BET}) and pore volume (V_{total}) compared to PC, as presented in Table 3. For instance, the PC had an S_{BET} of $2061.3 \text{ m}^2 \cdot \text{g}^{-1}$ and V_{total} of $0.95 \text{ cm}^3 \cdot \text{g}^{-1}$, whereas NPPC achieved an ultrahigh S_{BET} of $2980.6 \text{ m}^2 \cdot \text{g}^{-1}$ and V_{total} of $1.24 \text{ cm}^3 \cdot \text{g}^{-1}$. The pore size distribution was well-balanced, with micropores ($\leq 2 \text{ nm}$) providing numerous adsorption sites, and mesopores (2 to 50 nm) facilitating ion diffusion (Zhang *et al.* 2025). An important aspect is that the mesopore ratio (V_{meso}/V_{total}) of NPPC can reach up to 24.2%, which enhances the mass transport efficiency.

Table 3. Pore Structure for PC and NPPC

| Samples | S_{BET} ($\text{m}^2 \cdot \text{g}^{-1}$) | V_{total} ($\text{cm}^3 \cdot \text{g}^{-1}$) | V_{micro} ($\text{cm}^3 \cdot \text{g}^{-1}$) | V_{meso} ($\text{cm}^3 \cdot \text{g}^{-1}$) | $V_{micro}/V_{total}(\%)$ | $V_{meso}/V_{total}(\%)$ |
|---------|---|--|--|---|---------------------------|--------------------------|
| PC | 2061.3 | 0.95 | 0.74 | 0.21 | 78.04 | 21.96 |
| NPPC | 2980.6 | 1.24 | 0.94 | 0.31 | 75.81 | 24.19 |

Crystal Structure and Defect Density

Figure 5a exhibits XRD patterns of NPPC and PC. These displayed amorphous carbon characteristics, with broad peaks at approximately 23° and 40° , corresponding to the (002) and (101) crystal planes of graphite, respectively. However, the XRD pattern of NPPC displayed a slightly weaker peak intensity, suggesting a lower degree of crystallinity due to N/P co-doping. Raman spectroscopy identified two distinct peaks (Fig. 5b): the D band, observed at around 1345 cm^{-1} and associated with structural defects and disorder; and the G band, present at around 1589 cm^{-1} and representing sp^2 hybridized graphitic carbon. The intensity ratio of D to G bands (I_D/I_G) can be employed to assess the graphitization degree, with NPPC and PC exhibiting the values of 1.02 and 0.97, respectively. A higher I_D/I_G value directly signifies an increase in structural defects with numerous functionalized surface active sites, suggesting that N/P co-doping introduces more defects and disordered structures, which correspond to active sites for ion adsorption and charge storage.

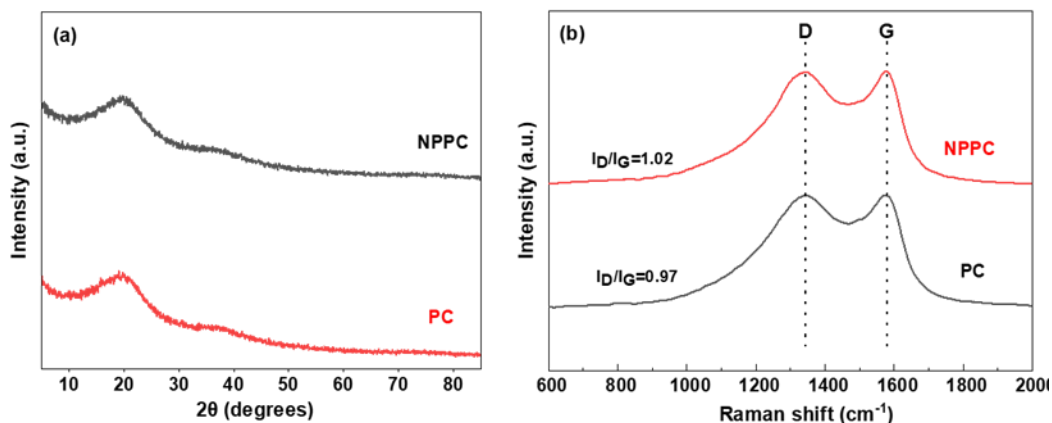


Fig. 5. (a) XRD patterns and (b) Raman spectroscopy results of PC and NPPC

Chemical Composition and Bonding Environment

The elemental composition of PC and NPPC was determined by XPS, and full spectrum plots are shown in Fig. 6a. Figure 6b shows that the high-resolution N 1s spectra of NPPC could be decomposed into various functional configurations, such as pyridinic N (around 398.3 eV), pyrrolic N (around 400.2 eV), and graphitic N (around 401.1 eV), with pyridinic N contributes to pseudocapacitance *via* Faradaic redox reactions. Pyrrolic N improves electrode wettability and graphitic N enhances the electrical conductivity of carbon materials. The P 2p spectrum (Fig. 6c) is divided into C–P bonds (around 132.2 eV) and P–O bonds (around 134.3 eV), with a larger peak area for C–P, suggesting a stable integration of P into the carbon matrix of NPPC.

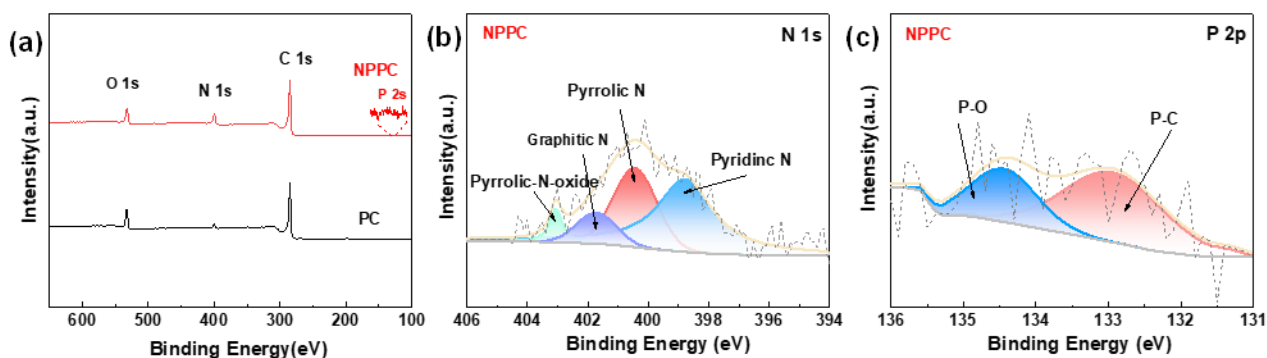


Fig. 6. XPS survey spectra of (a) PC and NPPC; and (b) N 1s and (c) P 2p spectra of NPPC

Table 4 presents the elemental content of PC and NPPC. Apparently, NPPC was characterized by intentional and effective co-doping of N and P heteroatoms into the carbon framework. NPPC exhibited a higher N content (12.33%) and P content (0.59%) than PC (4.79% and 0.03%, respectively). These findings indicate that NPPC exhibited lower charge transfer resistance, which can be attributed to the hierarchical porous structure and efficient N/P co-doping. These heteroatoms can introduce active sites on the surface of the carbon material, promoting redox reactions and thereby enhancing the contribution of pseudocapacitance (Chen *et al.* 2025).

Table 4. Elemental Contents of PC and NPPC

| Samples | C at. % | N at. % | O at. % | P at. % |
|---------|---------|---------|---------|---------|
| PC | 80.23 | 4.79 | 14.95 | 0.03 |
| NPPC | 76.58 | 12.33 | 10.50 | 0.59 |

CONCLUSIONS

To address the high-value utilization of traditional Chinese medicine (TCM) solid waste and the demand for sustainable high-performance electrode materials in supercapacitors, this work focuses on the development of N,P co-doped porous carbon (NPPC) using *Poria cocos* residue as the renewable carbon precursor. Through a facile single-batch carbonization-activation strategy with K_2CO_3 as the activator and melamine phosphate as the dual N/P dopant, combined with Box-Behnken design (BBD)-based response surface methodology (RSM) for precise parameter optimization, we successfully fabricated a hierarchical porous carbon material with exceptional electrochemical properties. The following conclusions are drawn based on systematic experimental investigations and characterizations:

1. A straightforward single-batch carbonization-activation approach was used to effectively fabricate N,P co-doped porous carbon materials from *Poria cocos* residues, thereby valorizing traditional Chinese medicine (TCM) residues and mitigating pollution. The key parameters were optimized through Box–Behnken design-based response surface methodology, identifying the optimal conditions as follows: a temperature of 580 °C, a K_2CO_3 ratio of 2.0, and an N,P co-doped ratio of 0.4. The optimized sample exhibited a superior electrochemical performance of 332 $F \cdot g^{-1}$ at 1 $A \cdot g^{-1}$ in 6 M KOH.
2. Synergistic K_2CO_3 activation and melamine phosphate doping enabled the formation of a highly optimized carbon material with a hierarchical porous structure, comprising both micropores and mesopores, and a uniform distribution of N (12.3%) and P (0.59%) heteroatoms. This resulted in enhanced active sites, improved ion diffusion, electronic structure tuning, and improved electrode wettability.
3. This cost-effective and environmentally sustainable approach provides a viable pathway for utilizing TCM residues, enabling the production of high-performance supercapacitor electrodes that can be extended to other types of biomass waste.

ACKNOWLEDGMENTS

The authors are grateful for the support of Youth Science Project of Guangxi (Grant No. 2023GXNSFBFA026289), Special Project for Young Innovative Talents in Project of Guangxi Science and Technology Base and Special Talent (Grant No. Guike AD22080019), Doctoral Foundation of Scientific Research Project of Wuzhou University (Green Construction and Electrochemical Performance of Carbon Film based on Chinese Medicine Residue, Grant No. 2022A001), Key Project of Wuzhou University (Design and Supercapacitive Performance of Biomass-Derived Carbon Materials/MXene Flexible Films, Grant No. 2024ZD005), Wuzhou Science and Technology Plan Project (Research

on Synergistic Removal of Binary Pollutants in Water by Magnetic Biomass Aerogels, Grant No. 202402027), and Education and Teaching Reform Project of Wuzhou University (Exploration and Practice of “Craftsman-type” Talent Training Mode in Applied Undergraduate Universities from the Perspective of Emerging Engineering Education, Grant No. Wyjg2023A053).

Use of Generative AI

The authors used Douba AI for literature organization in the introduction section and MogoEdit (<https://www.mogoedit.com>) for its English editing during the preparation of this manuscript.

REFERENCES CITED

- Alslaibi, T. M., Abustan, I., Ahmad, M. A., and Foul, A. A. (2013). “Cadmium removal from aqueous solution using microwaved olive stone activated carbon,” *J. Environ. Chem. Eng.* 1(3), 589-599. <https://doi.org/10.1016/j.jece.2013.06.028>
- Chen, C., Yang, L., Zhang, X., Zhao, C., Sun, J., Li, G., and Shi, H. (2024). “Advances and prospects of multifunctional biochar-based materials from organic solid waste of traditional Chinese medicine: A review,” *Biomass and Bioenergy* 187, article 107296. <https://doi.org/10.1016/j.biombioe.2024.107296>
- Chen, H., Lv, T., Guo, J., Wang, L., Li, L., Zhang, L., Li, P., Wang, C., and Zhu, L. (2025). “Self-doped porous carbon derived from traditional Chinese medicine residues for high performance supercapacitors,” *Industrial Crops and Products* 236, article 122055. <https://doi.org/10.1016/j.indcrop.2025.122055>
- Cheng, X., Zhang, L., Li, L., Li, X., Wu, H., Zheng, J., Yao, J., and Li, G. (2024). “One-step production of peanut shell derived N, P co-doped carbon materials for high-performance symmetric supercapacitors,” *Colloids and Surfaces A: Physicochemical and Engineering Aspects* 698, article 134542. <https://doi.org/10.1016/j.biombioe.2024.107296>
- Huang, J., Chen, J., Yin, Z., and Wu, J. (2020). “A hierarchical porous P-doped carbon electrode through hydrothermal carbonization of pomelo valves for high-performance supercapacitors,” *Nanoscale Advances* 2(8), 3284-3291. <https://doi.org/10.1039/d0na00211a>
- Hung, P., Zhang, H., Lin, H., Guo, Q., Lau, K. T., and Jia, B. (2022). “Specializing liquid electrolytes and carbon-based materials in EDLCs for low-temperature applications,” *Journal of Energy Chemistry* 68, 580-602. <https://doi.org/10.1016/j.jechem.2021.12.012>
- Jia, L., Yu, G., Qin, Z., Wang, G., Ruan, D., and Tu, J. (2025). “The performance analysis of supercapacitors utilizing chemically activated carbon derived from Chinese medicine residues,” *Biomass Conversion and Biorefinery* 15(9), 13783-13796. <https://doi.org/10.1007/s13399-024-06028-9>
- Kang, J., Atashin, S., Jayaram, S. H., and Wen, J. Z. (2017). “Frequency and temperature dependent electrochemical characteristics of carbon-based electrodes made of commercialized activated carbon, graphene and single-walled carbon nanotube,” *Carbon* 111, 338-349. <https://doi.org/10.1016/j.carbon.2016.10.017>
- Li, G., Li, Y., Chen, X., Hou, X., Lin, H., and Jia, L. (2022). “One step synthesis of N, P co-doped hierarchical porous carbon nanosheets derived from pomelo peel for high

- performance supercapacitors,” *Journal of Colloid and Interface Science* 605, 71-81. <https://doi.org/10.1016/j.jcis.2021.07.065>
- Liu, S., Dong, K., Guo, F., Wang, J., Tang, B., Kong, L., Zhao, N., Hou, Y., Chang, J., and Li, H. (2024). “Facile and green synthesis of biomass-derived N, O-doped hierarchical porous carbons for high-performance supercapacitor application,” *Journal of Analytical and Applied Pyrolysis* 177, article 106278. <https://doi.org/10.1016/j.jaap.2023.106278>
- Liu, X., Gao, Q., Cheng, X., Li, L., Zhang, L., Wu, H., Zhang, L., Zheng, J., Li, J., and Gao, H. (2026). “Acid and alkali jointly promote the co-doping of N, B and O atoms in wheat straw derived carbon materials for high-performance symmetrical supercapacitors,” *Fuel* 403, article 136102. <https://doi.org/10.1016/j.fuel.2025.136102>
- Murugan, N., Thangarasu, S., Seo, S. B., Mariappan, A., Choi, Y. R., Oh, T. H., and Kim, Y. A. (2024). “N-doped defect-rich porous carbon nanosheets framework from renewable biomass as efficient metal-free bifunctional electrocatalysts for HER and OER application,” *Renewable Energy* 222, article 119801. <https://doi.org/10.1016/j.renene.2023.119801>
- Qiang, H., Shi, M., Wang, F., and Xia, M. (2024). “Biomass-based N/P co-doped hierarchical porous carbon fabricated by a facile dual physico-chemical activation strategy for efficient capacitive deionization,” *Separation and Purification Technology* 333, article 125915. <https://doi.org/10.1016/j.seppur.2023.125915>
- Shi, M., Lu, K., Hong, X., Qiang, H., Liu, C., Ding, Z., Wang, F., and Xia, M. (2023). “High-yield green synthesis of N-doped hierarchical porous carbon by nitrate-mediated organic salt activation strategy for capacitive deionization: Universality and commerciality,” *Chemical Engineering Journal* 471, article 144465. <https://doi.org/10.1016/j.cej.2023.144465>
- Tahir, N., Ramzan, H., Nadeem, F., Usman, M., Shahzaib, M., Rahman, M. U., Liu, Y., Afzal, W., Lam, S. S., and Zhang, Z. (2026). “Engineering the microbial-electrochemical interface: Synergistic of co-fe nano biochar composites for enhanced electron channelling to alter the metabolic pathway in light-driven biohydrogen production,” *Biochar* 8(1), article 31. <https://doi.org/10.1007/s42773-025-00539-y>
- Teimouri, Z., Nanda, S., Abatzoglou, N., and Dalai, A. K. (2024). “Application of activated carbon in renewable energy conversion and storage systems: A review,” *Environmental Chemistry Letters* 22(3), 1073-1092. <https://doi.org/10.1007/s10311-023-01690-3>
- Tiwari, S. K., Bystrzejewski, M., De Adhikari, A., Huczko, A., and Wang, N. (2022). “Methods for the conversion of biomass waste into value-added carbon nanomaterials: Recent progress and applications,” *Progress in Energy and Combustion Science* 92, article 101023. <https://doi.org/10.1016/j.jcis.2021.07.065>
- Wang, J., Huo, T., Zhao, Y., Lu, R., and Wu, X. (2025). “Recent advances in hetero-atoms-doped porous carbon electrode materials for supercapacitors: A review,” *Journal of Energy Storage* 110, article 115216. <https://doi.org/10.1016/j.ccr.2025.216949>
- Wang, X., Zhang, H., Zhang, J., Xu, H., Tian, Z., Chen, J., Zhong, H., Liang, Y., and Yi, B. (2006). “Micro-porous layer with composite carbon black for PEM fuel cells,” *Electrochimica Acta* 51(23), 4909-4915. <https://doi.org/10.1016/j.electacta.2006.01.048>

- Wang, Y., Zhang, M., Dai, Y., Wang, H.-Q., Zhang, H., Wang, Q., Hou, W., Yan, H., Li, W., and Zheng, J.-C. (2019). "Nitrogen and phosphorus co-doped silkworm-cocoon-based self-activated porous carbon for high performance supercapacitors," *Journal of Power Sources* 438, article 227045. <https://doi.org/10.1016/j.jpowsour.2019.227045>
- Wu, C., Liu, J., Wu, W., Wang, Y., Zhao, Y., Li, G., Zhang, Y., and Zhang, G. (2025). "Mild modification of sponge-like carbon: Ammonia post-treatment for enhanced CO₂ adsorption and suitability for supercapacitors," *Separation and Purification Technology* 353, article 128525. <https://doi.org/10.1016/j.seppur.2024.128525>
- Yan, L., Yu, J., Houston, J., Flores, N., and Luo, H. (2017). "Biomass derived porous nitrogen doped carbon for electrochemical devices," *Green Energy & Environment* 2(2), 84-99. <https://doi.org/10.1016/j.gee.2017.03.002>
- Yan, X., Yu, Y., and Yang, X. (2014). "Effects of electrolytes on the capacitive behavior of nitrogen/phosphorus co-doped nonporous carbon nanofibers: An insight into the role of phosphorus groups," *RSC Advances* 4(48), 24986-24990. <https://doi.org/10.1039/c4ra02299h>
- Yuan, Y., Wei, L., Sun, X., and Sun, G. (2024). "Optimization of deep eutectic-like solvent-based ultrasound-assisted extraction of polysaccharides from *Leonurus* residues," *BioResources* 19(2), 2299-2313. <https://doi.org/10.15376/biores.19.2.2299-2313>
- Zhai, Y., Xu, B., Zhu, Y., Qing, R., Peng, C., Wang, T., Li, C., and Zeng, G. (2016). "Nitrogen-doped porous carbon from *Camellia oleifera* shells with enhanced electrochemical performance," *Materials Science and Engineering: C* 61, 449-456. <https://doi.org/10.1016/j.msec.2015.12.079>
- Zhang, W., Ma, T., and Li, M. (2025). "Fabrication of an ultrasensitive electrochemical sensor using Fe-NS tri-doped MWCNTs for simultaneous determination of catechol and hydroquinone," *Microchemical Journal*, article 114869. <https://doi.org/10.1016/j.microc.2025.114869>
- Zhang, X., Wang, Y., Yu, X., Tu, J., Ruan, D., and Qiao, Z. (2021). "High-performance discarded separator-based activated carbon for the application of supercapacitors," *Journal of Energy Storage* 44, article 103378. <https://doi.org/10.1016/j.est.2021.103378>
- Zhou, Q., Li, H., Jia, B., Dang, Y., and Zhang, G. (2023). "One-pot synthesis of porous carbon from Chinese medicine residues driven by potassium citrate and application in supercapacitors," *Journal of Analytical and Applied Pyrolysis* 170, article 105894. <https://doi.org/10.1016/j.jaap.2023.105894>

Article submitted: March 11, 2026; Peer review completed: May 3, 2026; Revised version received and accepted: May 5, 2026; Published: May 18, 2026.

DOI: 10.15376/biores.21.3.6068-6082